Icarus 238 (2014) 230–234

Contents lists available at ScienceDirect

Icarus

journal homepage: www.elsevier.com/locate/icarus

Note

Revisited modeling of Titan's middle atmosphere electrical conductivity

Alabhya Mishra [a], Marykutty Michael [a], Sachchida Nand Tripathi [a,*], Christian Béghin [b]

[a] Department of Civil Engineering, Indian Institute of Technology Kanpur, Kanpur, India
[b] LPC2E-CNRS-Université d'Orléans, 3A, Ave. Recherche Scientifique, 45071 Orléans Cedex 2, France

ARTICLE INFO

Article history:
Received 5 September 2013
Revised 24 March 2014
Accepted 16 April 2014
Available online 9 May 2014

Keywords:
Titan
Satellites, atmospheres
Saturn, satellites
Cosmic rays

ABSTRACT

The atmospheric electrical conductivity measured by the Permittivity, Wave and Altimetry (PWA) subsystem on board the Huygens probe, during the landing mission on Titan, has been modeled in the present work. Previous modeling studies showed a Galactic Cosmic Ray (GCR) peak of conductivity at a higher altitude and a quantitative overestimation in the altitude range 0–100 km compared to that observed by the PWA instrument. Recently the PWA data was revisited and provided new constraints on the conductivity at altitudes 100–180 km. Because the aerosols in the atmosphere are known to alter the electron concentration, using a detailed distribution of the aerosols at all altitudes, the electron conductivity has been calculated in the altitude range 0–180 km. By using a variable range of photoemission threshold for the aerosols, the present model is able to reasonably predict the altitude at which the GCR peak of conductivity occurs and to meet the new constraints for the conductivity profile.

1. Introduction

The electron conductivity results from the presence of free electrons in planetary atmospheres. At night time, the attachment of electrons to the aerosol substantially reduces the electron abundance and thus the conductivity. However during daytime solar ultraviolet radiation impinging on the aerosol particles causes emission of electrons, leaving the particles with positive charge and greatly increasing the electron conductivity. Through photoemission from embryos and negative ions as well as ionization of molecules by Galactic Cosmic Rays (GCR), there is further addition to the free electron concentration in the atmosphere along with the formation of positive ions (Borucki et al., 2006). An interaction between all of these charge carrying species, as well as neutral aerosols, occurs in the atmosphere. These interactions involve loss of electrons by recombination with positive ions, attachment with neutral as well as charged aerosols, formation of negative ions by attachment of electron to neutral embryos and attachment with positively charged embryos. Further interactions amongst positive ions, negative ions and aerosols are also an integral part of the aerosol charging process occurring in the atmosphere. These interactions are important to the prediction of electron densities as well as inhibition of coagulation of aerosols. Inhibition in coagulation of aerosols is important as these favors the presence of larger concentrations of smaller particles, and thus affect the vertical deposition of solar flux. This in turn affects the rate of photoemission of electrons in the atmosphere.

Fulchignoni et al. (2005) and Hamelin et al. (2007) reported the electrical measurements made using the PWA subsystem, which is a component of the Huygens Atmospheric Structure Instrument (HASI) during the Huygens probe landing at Titan. PWA detected an ionized layer in the altitude region of 50–80 km, attributed mainly to GCRs, with a maximum conductivity at around 60–65 km, although the previous models (Molina-Cuberos et al., 1999; Borucki et al., 1987, 2006) predicted instead a peak at higher altitude, at around 90–100 km. The altitude profile of conductivity and electron concentration were also observed from 100 km down to the surface by the PWA instrumentation (Hamelin et al., 2007), but the measurements were not in agreement with the existing models. These disagreements could be caused by a wrong estimate of the electron attachment to different kinds of aerosol layers. Borucki and Whitten (2008) estimated the conductivity in the altitude range 0–150 km keeping constraints of abundance and size of the aerosols deduced from the Huygens probe measurements. Tomasko et al. (2005) reported that the size and the concentration of aerosols may be independent of altitude, which is an unexpected explanation. Borucki and Whitten (2008) obtained the size and abundance distribution by assuming constant mass flux with altitude and measured optical depth as a constraint. However, the conductivity profile calculated by Borucki and Whitten (2008) was not in agreement with PWA data, except for altitudes 50–55 km.

In this paper a model has been developed based on previous works by Michael et al. (2007, 2008, 2009). The conductivity in our current model has been computed for the altitude range of 0–180 km and has been compared to the values observed below 100 km and also fitted to the constraints applied to higher altitudes regions determined by Béghin et al. (2012) and Béghin (2014). Although previous models have not been able to simulate these profiles, we have been able to make significant progress in this direction by adjusting certain parameters, especially the photoemission threshold (Borucki and Whitten, 2008) with some assumptions.

2. General description of the model

In this model, the atmospheric electron conductivity and the electrical charges of the aerosols in the altitude range from 0 to 180 km are estimated from steady-state calculations, based on first, the ionization due to the absorption of high-energy particles by atmospheric gases, and second, the solar UV radiation on the aerosols, followed by the recombination of ions and electrons. The required inputs to the model are the vertical profile of temperature, pressure, ion pair production rate and aerosol size distribution, as well as number density concentration. Temperature and pressure profiles were obtained from the HASI data file, whereas the aerosol size distribution was provided by Lavvas through personal communication (the details about the model is provided in Lavvas et al. (2008)). The ion pair production rates have been treated in detail by Gronoff et al. (2009). Solar fluxes used for the calculation of the photoionization of aerosols were scaled for Titan using the data provided by Huebner et al. (1992).

* Corresponding author. Address: Department of Civil Engineering, Indian Institute of Technology Kanpur, Kanpur, UP 208016, India. Fax: +91 512 2597395.
E-mail addresses: alabhya@iitk.ac.in (A. Mishra), mary@iitk.ac.in (M. Michael), snt@iitk.ac.in (S.N. Tripathi), christian.beghin@cnrs-orleans.fr (C. Béghin).

http://dx.doi.org/10.1016/j.icarus.2014.04.018
0019-1035/

2.1. Photoionization of aerosols

Apart from the electron produced from absorption of GCR by the gaseous species of the atmosphere, there is a significant contribution during day time by photoemission from the aerosols due to solar UV radiation of wavelength greater than 150 nm.

Aerosols in the atmosphere of Titan exist as aggregates of smaller particles. A detailed explanation of such aggregates is provided in Tomasko et al. (2008). In the present study we have used the Discrete Dipole Approximation (DDScat ver 7.3) to compute the extinction and scattering efficiencies. The refractive indices were taken from Tran et al. (2003). The attenuated intensity is then calculated using the 2 stream Radiative-Transfer model as follows:

$$\frac{d\varphi^{+}(z,\lambda)}{dz} + (\sigma_{ext})N(z)\varphi^{+}(z,\lambda) = N(z)\sigma_{scat}\varphi^{-}(z,\lambda) \quad (1)$$

$$\frac{d\varphi^{-}(z,\lambda)}{dz} - (\sigma_{ext})N(z)\varphi^{-}(z,\lambda) = -N(z)\sigma_{scat}\varphi^{+}(z,\lambda) \quad (2)$$

where $\varphi^{+}(z,\lambda)$ and $\varphi^{-}(z,\lambda)$ are the downward and upward solar fluxes, $N(z)$ is the number concentration of aerosols and σ_{ext} and σ_{scat} are respectively the extinction and scattering cross-sections of the aerosols. The relationships between the cross-sections and the efficiencies are described by Moosmüller et al. (2009). To account for the poly disperse nature (i.e. a distribution of aerosols is used at each altitude instead of an equivalent size at each altitude) of aerosols, following relations were used in the calculation of extinction and scattering cross sections of an ensemble of particles:

$$(\sigma_{ext})N(z) = \int_{D_{p,min}}^{D_{p,max}} \frac{\pi D_p^2}{4} Q_{ext} n(D_p) dD_p \quad (3)$$

$$(\sigma_{scat})N(z) = \int_{D_{p,min}}^{D_{p,max}} \frac{\pi D_p^2}{4} Q_{scat} n(D_p) dD_p \quad (4)$$

Here $D_{p,max}$ is the maximum size of the particle and $D_{p,min}$ the minimum; Q_{ext}, and Q_{scat} are the extinction and scattering efficiencies; $n(D_p)$ denotes the concentration of aerosols of particle size D_p. The photoelectric ejection rate from aerosols is then calculated as:

$$q_e = \int_{\lambda}^{th} W(z)\sigma_x(\lambda)d\lambda \quad (5)$$

Here $W(z)$ is the attenuated solar intensity at altitude z, σ_x is the ionization cross-section of aerosol. The integration was performed within required limits of wavelengths. The lower limit wavelength was fixed at 150 nm whereas the threshold wavelength varied, as required for calculation, from 170 nm to 207 nm.

2.2. Photoionization of embryos and negative ions

Embryos were introduced in our model for altitudes above 80 km. Embryos are very small particles ($\sim 7 \times 10^{-4}$ μm) but possess a higher mobility with respect to the atmosphere. These small particles can be fullerenes or Polycyclic Aromatic Hydrocarbons (PAH). Sittler et al. (2009) reported that the existence of fullerenes and PAH is possible in the atmospheric conditions of Titan. The concentration of embryos is 97.9 cm^{-3} at 80 km. It increases with altitude and peaks in the altitude range 100–120 km with a concentration of 1.38×10^3 cm^{-3}. Then the concentration decreases with altitude and becomes 789.6 cm^{-3} at 150 km. Since they have the same composition as the aerosols, they too contribute to the photoemission of electrons. However owing to small size, higher mobility as well as an electrophilic nature, electrons when attach to embryos they can behave as negative ions in the atmosphere. Photoionization of embryos as well as negative ions were included in the model. However taking into account the very small size of embryos, Mie Theory was no longer applicable. Thus we resorted to the Rayleigh scattering regime for calculation of scattering and extinction coefficients. Since embryos are equivalent to aerosols in all properties except size, threshold of photoionization remains unchanged. But the presence of negative charge on embryos is likely to decrease its threshold of photoionization, thus an upper limit of 600 nm (2.07 eV; see Table 3, Borucki et al., 2006) was used in Eq. (5) for the calculation of the photo electron ejection rate.

2.3. Steady state ion and electron concentration

The steady state concentrations of ions and electrons are calculated using the following charge balance equations:

$$\frac{dn_e}{dt} = q_e + q + q_{emb} + q_{neg} - \alpha_e n_e n_+ - \beta_{emb} n_{emb} n_e - \beta^{+}_{emb} n^{+}_{emb} n_e - n_e \sum_i \sum_k \beta^i_{ek} N^i_k \quad (6)$$

$$\frac{dn_-}{dt} = \beta_{emb} n_{emb} n_e - q_{neg} - \alpha n_+ n_- - n_- \sum_i \sum_k \beta^i_{2k} N^i_k \quad (7)$$

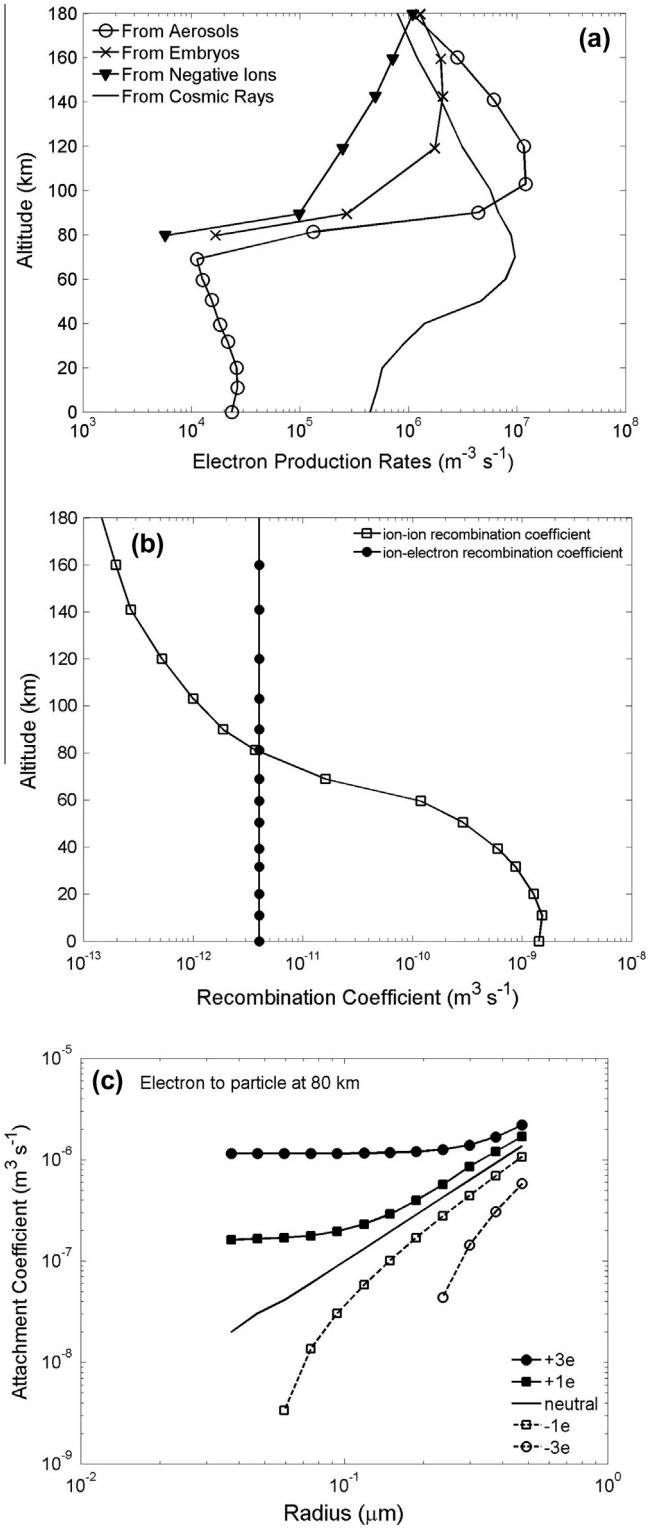

Fig. 1. (a) Electron production rates from different sources, (b) ion–ion and ion–electron recombination coefficient, and (c) electron–aerosol attachment coefficient at 80 km.

$$\frac{dn_+}{dt} = q - \alpha n_+ n_- - \alpha_e n_+ n_e - n_+ \sum_i \sum_k \beta^i_{1k} N^i_k \quad (8)$$

$$\frac{dn^{+}_{emb}}{dt} = q_{emb} - \beta^{+}_{emb} n^{+}_{emb} n_e \quad (9)$$

where n_e, n_- and n_+ are the concentrations of electron, negative ions and positive ions respectively, n_{emb} the concentration of embryos and n^{+}_{emb} is the concentration

Table 1
Concentration (m^{-3}) of charged and neutral particles (radii 0.07 μm and 0.15 μm) at two representative altitudes 80 km and 120 km.

Radius of the particle (μm)	Concentration of particles carrying different charges				
	−1*e*	0*e*	1*e*	2*e*	3*e*
At altitude 80 km					
0.07	2.19E−04	4.36E+00	1.02E+04	1.66E+06	0
0.15	1.90E−06	1.93E−02	8.74E+01	9.84E+04	1.36E+07
At altitude 120 km					
0.07	6.69E−04	6.30E+00	1.35E+04	3.18E+06	0
0.15	2.80E−06	1.62E−02	5.57E+01	6.70E+04	1.74E+07

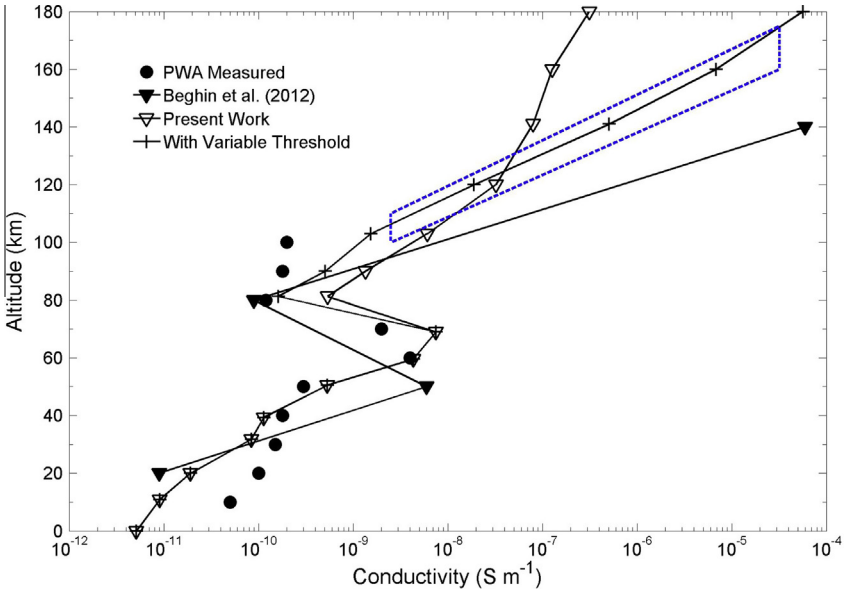

Fig. 2. Comparison of our model (open triangles) between the PWA measurements of conductivity (circles) and the initial constraints (triangles) by Béghin et al. (2012). This electron conductivity profile was produced for a threshold of photoionization fixed at 6.6 eV for aerosols and embryos and 2.07 eV for negative ions. Even though the change in slope at 80 km altitude reproduces the trend of the PWA measurements, actual values are off by up to an order of magnitude for altitudes above 80 km and below 30 km. Also the lack of reliable measurements above 100 km poses a difficulty in characterizing the conductivity at higher altitudes. Revised conductivity profile (crosses and dotted blue outlined quadrilateral) with revisited constraints by Béghin (2014). Here, different photoemission threshold of aerosols are considered (i.e., 6.6 eV below 80 km, 7.0 eV at 80 km, 6.9 eV at 90 km, 6.8 eV at 100 km, 6.6 eV at 120 km, 6.4 eV at 140 km, 6.0 eV at 160 km, and 5.7 eV at 180 km). (For interpretation of the references to color in this figure legend, the reader is referred to the web version of this article.)

of embryos carrying positive charge. Electron production rates by photoionization are q_e from aerosols, q_{emb} from embryos and q_{neg} from negative ions. Also q is the ion pair production rate from cosmic ray secondaries. Fig. 1a shows the comparison of various electron production rates, q, q_e, q_{emb}, and q_{neg}. α_e is the recombination coefficient for electron and positive ions, and α is the recombination coefficient for negative ions and positive ions. Fig. 1b provides the altitude profiles of α and α_e. Other terms being β_{emb} the electron to embryo attachment coefficient, β^+_{emb} the electron to positively charged embryo attachment coefficient, N^i_k the concentration of aerosols of charge index i and radius index k, β^i_{mk} the species to aerosol attachment coefficient, subscript (m) as e, 1 and 2 refer to electron, positive ion and negative ion species respectively. Fig. 1c provides the electron–aerosol attachment coefficients at 80 km.

Both β_{emb} and β^+_{emb} were calculated in the same way as β^i_{mk}. Conservation for total number of embryos requires the restriction $n^{init}_{emb} = n_{emb} + n_- + n^+_{emb}$, where n^{init}_{emb} is the total initial uncharged embryo concentration. Also charge conservation was imposed on total charge at every altitude as $\sum_p pN_p - n_e - n_- + n_+ + n^+_{emb} = 0$, where N_p is the concentration of aerosol carrying charge p. Finally, electron conductivity ($\sigma_e = en_e\mu_e$) is computed. Here $e = 1.60217646 \times 10^{-19}$ is the elementary charge and n_e and μ_e are the steady state concentration and mobility of electrons respectively. Electron mobility has been calculated using the equations provided in Borucki et al. (1987) and Banks and Kockarts (1973) to account for a Nitrogen rich atmosphere of Titan. Electron mobility is 50 $m^2\,V^{-1}\,s^{-1}$ at 80 km and increases to 550 $m^2\,V^{-1}\,s^{-1}$ in the atmosphere. The concentration of neutral and charged aerosols at two altitudes is shown in Table 1.

3. Results and discussion

Actual measurements of electron conductivity of Titan's atmosphere were performed during the Huygens probe descent in January 2005, by the PWA instrument (Hamelin et al., 2007). These measurements show a significant decrease in conductivity values below 60 km, but previous models of Titan's electron conductivity were not able to simulate this sudden drop.

However, Fig. 2 shows that we were able to achieve this trend through our model. We believe that this effect can be attributed to the introduction of embryos at that altitude which leads to loss of electron by formation of negative ions. The presence of embryos leads to formation of negative ions. Since these ions are formed by attachment of electrons to embryos, there is a higher loss in the steady state concentration of electrons at 80 km as compared to 70 km, resulting in the apparent bump observed. It should be noted that embryos as well as negative ions also contribute to an increase in electron production rate through their own photoionization. However the solar radiation reaching altitudes of 80 km are so small (<10% of incident radiation) that such a contribution is almost negligible for lower altitudes. The increasing effect of contribution from embryos and negative ions can, nevertheless, be seen at higher altitudes, where a very high percentage of solar radiation can reach (~70% of incident radiation at 150 km).

There are several irregularities in the nature of aerosols in the atmosphere of Titan, perhaps associated with aerosols layers of different nature, size and density. Keeping this uncertainty in mind, we concede that true conductivity cannot be modeled at this stage. We can however tweak with certain parameters, either the input variable or involved processes to a certain extent, to try and close the gap between the known measurements of conductivity and those that are modeled. So we performed several sensitivity analyses on our model to create a set of variables that affected the resulting conductivity the most. It was seen during these analyses that our model was not very sensitive to parameters like temperature, pressure and size of aerosols. The most sensitive parameters were the threshold of photoionization and the number concentration of aerosols. Since we did not have much data on the variation in number concentration (with polydisperse distribution at each altitude) of aerosols we decided to regulate the threshold of photoionization to see if we could achieve the desired conductivity values at certain altitudes. This direction

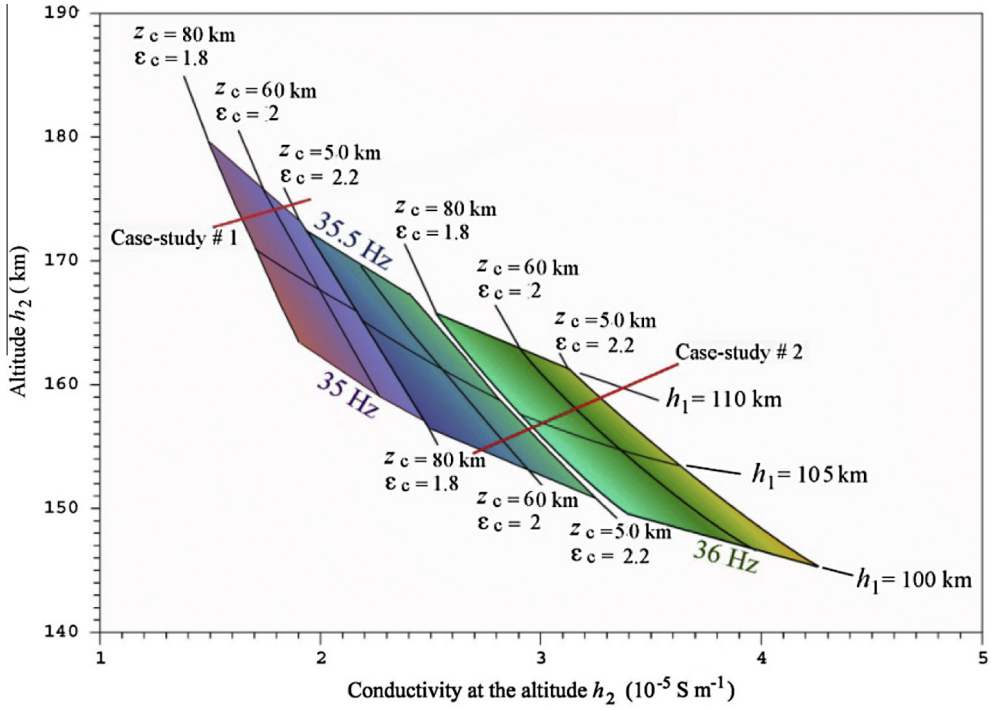

Fig. 3. Summary chart of revisited cross-constrained Titan's atmospheric and icy-crust Schumann cavity parameters: i.e., crust thickness and permittivity (z_c and ε_c), bound altitude h_1 and frequency of the second Schumann mode frequency (35, 35.5 and 36 Hz) plotted versus the altitude and the conductivity of h_2, for two case-studies fitting the new conductivity profile (Fig. 2, blue quadrilateral) with the PWA data.

to our work gained confidence from the fact that several studies of this nature were previously done (Béghin et al., 2012; Borucki and Whitten, 2008). More recently, a new conductivity profile above 100 km was proposed using revisited constraints (Béghin, 2014), as described in further detail in Section 3.1.

3.1. Constraining the electron conductivity above 100 km altitude

The PWA instrumentation measured the Extra Low Frequency (ELF) natural waves, the most significant of which has been interpreted as a second eigenmode of an atypical Schumann Resonance (SR) within the cavity lying between the lower ionosphere and the conductive water ocean buried under few tens of kilometers thickness of the icy crust (Béghin et al., 2012). Starting from measured spectral characteristics of the PWA signal around the 36 Hz peak amplitude, the parameters of the entire cavity are constrained by the following theoretical modal equations:

$$\omega_l = \frac{c}{a}\left[l(l+1)\frac{h_1 + z_C/R_e\varepsilon_c}{h_2 + z_c}\right]^{1/2}\left[1 - i\left(\frac{z_C\delta/R_e\varepsilon_c + \pi\zeta/4}{h_1 + z_C/R_e\varepsilon_c} + \frac{\pi\zeta/4}{h_2 + z_c}\right)\right] \quad (10)$$

$$Q_l = \left|\frac{R_e}{2I_m f_l}\right| = \left[\frac{2z_C\delta/R_e\varepsilon_c + \pi\zeta/2}{h_1 + z_C/R_e\varepsilon_c} + \frac{\pi\zeta/2}{h_2 + z_c}\right]^{-1} \quad (11)$$

where $\omega_l = 2\pi f_l$ is the complex angular frequency for any eigenmode of degree l, and Q_l is the associated quality factor (a real quantity); c is the free-space light velocity and a the Titan's mean radius (~2575 km), h_1 and h_2 are the altitudes of the conduction and diffusion bounds respectively, within the atmospheric portion of the cavity, ζ is the average scale height of the electron conductivity from h_1 up to h_2, assuming a smoothed exponential law in between, and z_c, ε_c and δ are the thickness, permittivity and loss tangent respectively, of the Titan's surface icy-crust. The symbols R_e and I_m are used for real and imaginary part of the quantities. A preliminary set of cross-constraints between these parameters has been proposed as to better fit the Huygens data (Béghin et al., 2012), assuming $f_2 = 36$ Hz and $Q_2 = 6$, corresponding to the bound values $h_1 \sim 100$ km and $h_2 \sim 140$ km with conductivities of $\sim 2 \times 10^{-9}$ and 2.5×10^{-5} S m^{-1} respectively. The icy crust thickness z_c was found between 50 km and 80 km, with a permittivity ε_c between 2 and 3.

More recently, these constraints have been revisited using a self-consistent sophisticated spectral analysis of the PWA data Béghin (2014). The new constraint parameters are essentially a significant increase of the upper diffusion altitude h_2 ranging from 145 to 165 km for the most likely case-studies (Fig. 3), and a possible adjustment of the altitude h_1 (100–110 km), keeping the same order of magnitude of conductivity ($\sim 2 \times 10^{-9}$ S m^{-1}) in that region. In addition, the new constraints do not imply a perfectly uniform exponential scale height of conductivity between both bounds, provided that the constrained values fit the bound altitudes.

3.2. Modeling the revisited constrained conductivity

The revisited SR constraints of conductivity are now about 2.5×10^{-9} S m^{-1} at around of 100–110 km, and $1.6–3.2 \times 10^{-5}$ S m^{-1} between 160 and 175 km, considering the most likely case-study models which fit the PWA data. Using these values we created the desirable range of conductivity for altitudes 100–170 km which is shown as a dotted blue outlined quadrilateral in Fig. 2. Many studies show that the composition of haze particles could be different at different altitudes and latitudes (Kok et al., 2007; Sittler et al., 2009; Rannou et al., 2010; Lavvas et al., 2013). Therefore, we checked several values of photoionization threshold for aerosols in order to fit the conductivities derived from our model within the constrained range reported by Borucki and Whitten (2008). We found that the range of expected conductivity fell within thresholds of photoionization from 177 nm (7.0 eV) to 217 nm (6.0 eV) respectively.

Borucki and Whitten (2008) inferred that the production of electrons from the photoemission of aerosols in the lower atmosphere of Titan is not an important process. However, the present work shows that, a more realistic aerosol distribution than those used by these authors and a variable threshold allowing control of aerosol photoemission and the production rate of electrons, can predict the altitude at which the maximum conductivity occurs and the trend of the conductivity profile. The present work also shows a better agreement between the electron conductivity and the observations, compared to the previous models.

4. Conclusions

The electrical conductivity in the lower atmosphere of Titan has been revisited in the present work because the conductivity profiles predicted by the previous models were not in agreement with the PWA observations, in the sense that they predicted a peak of conductivity at 90–100 km whereas the measurements showed a GCR peak conductivity at 60–65 km. Using a more realistic distribution of aerosols, our model may account for the measured value of conductivity, at the same peak altitude. The present work also shows that the production of electrons by the photoemission of aerosols is an important process in the lower atmosphere of Titan. Furthermore, as suggested by Borucki and Whitten (2008) and Béghin et al. (2012), we consider an altitude varying threshold of photoionization, within the limits (6.0–7.0 eV), from 80 km to 160 km. By feeding these new parameter values to our model we have extended the electron conductivity profile up to altitudes greater than 100 km, in order to comply with the revisited SR constraints reported by Béghin (2014). Better agreement with PWA electron conductivity measurements below 100 km (Hamelin et al., 2007) was also achieved.

Acknowledgments

This work was initiated after the invitation by Dr. Tagger Director of LPC2E-University of Orleans for a two months position to SNT as a guest visiting professor. MM acknowledges support through the DST Fast-Track Fellowship. SNT gratefully acknowledges the financial support given by the Earth System Science Organization, Ministry of Earth Sciences, Government of India to conduct this research.

References

Banks, P.M., Kockarts, G., 1973. Aeronomy. Elsevier Science & Technology Books, ISBN-13: 9780120778027.

Béghin, C., 2014. The atypical generation mechanism of Titan's Schumann Resonance. J. Geophys. Res.: Planets 119. http://dx.doi.org/10.1002/2013JE004569.

Béghin, C. et al., 2012. Analytic theory of Titan's Schumann Resonance: Constraints on ionospheric conductivity and buried water ocean. Icarus 218, 1028–1042.

Borucki, W.J., Whitten, R.C., 2008. Influence of high abundances of aerosols on the electrical conductivity of the Titan atmosphere. Planet. Space Sci. 56, 19–26. http://dx.doi.org/10.1016/j.pss.2007.03.013.

Borucki, W.J. et al., 1987. Predictions of the electrical conductivity and charging of the aerosols in Titan's atmosphere. Icarus 72, 604–622.

Borucki, W.J., Whitten, R.C., Bakes, E.L.O., Barth, E., Tripathi, S.N., 2006. Predictions of the electrical conductivity and charging of the aerosols in Titan's atmosphere. Icarus 72 (1987), 604–622, ISSN 0019-1035.

Fulchignoni, M. et al., 2005. In situ measurements of the physical characteristics of Titan's environment. Nature 438, 785–791. http://dx.doi.org/10.1038/nature04314.

Gronoff et al., 2009. Ionization processes in the atmosphere of Titan. I. Ionization in the whole atmosphere. Astron. Astrophys. http://dx.doi.org/10.1051/0004-6361/200912371.

Hamelin, M. et al., 2007. Electron conductivity and density profiles derived from the mutual impedance probe measurements performed during the descent of Huygens through the atmosphere of Titan. Planet. Space Sci. 55, 1964–1977. http://dx.doi.org/10.1016/j.pss.2007.04.008.

Huebner, W.F., Keady, J.J., Lyon, S.P., 1992. Solar photo rates for planetary atmospheres and atmospheric pollutants. Astrophys. Space Sci. 195, 1–294.

Kok, R.D., Irwin, P.G.J., Teanby, N.A., Nixon, C.A., Jennings, D.E., Fletcher, L., Howett, C., Calcutt, S.B., Bowles, N.E., Flasar, F.M., Taylor, F.W., 2007. Characteristics of Titan's stratospheric aerosols and condensate clouds from Cassini CIRS far-infrared spectra. Icarus 191, 223–235.

Lavvas, P., Coustenis, A., Vardavas, I.M., 2008. Coupling photochemistry with haze formation in Titan's atmosphere, part II: Results and validation with Cassini/Huygens data. Planet. Space Sci. 56, 67–99. http://dx.doi.org/10.1016/j.pss.2007.05.027.

Lavvas, P. et al., 2013. Aerosol growth in Titan's ionosphere. Proc. Natl. Acad. Sci. http://dx.doi.org/10.1073/pnas.1217059110.

Michael, M., Barani, M., Tripathi, S.N., 2007. Numerical predictions of aerosol charging and electrical conductivity of the lower atmosphere of Mars. Geophys. Res. Lett. 34, L04201. http://dx.doi.org/10.1029/2006GL028434.

Michael, M., Tripathi, S.N., Mishra, S.K., 2008. Dust charging and electrical conductivity in the day and night-time atmosphere of Mars. J. Geophys. Res. 113, E07010. http://dx.doi.org/10.1029/2007JE003047.

Michael, M., Tripathi, S.N., Borucki, W.J., Whitten, R.C., 2009. Highly charging of particles by ion attachment in the atmosphere of Venus. J. Geophys. Res. 114, E04008. http://dx.doi.org/10.1029/2008JE003258.

Molina-Cuberos, G.J., Ló pez-Moreno, J.J., Rodrigo, R., Lara, L.M., 1999. Chemistry of the Galactic Cosmic Ray induced ionosphere of Titan. J. Geophys. Res. 104 (E9), 21997–22024. http://dx.doi.org/10.1029/1998JE001001.

Moosmüller, H., Chakrabarty, R.K., Arnott, W.P., 2009. Aerosol light absorption and its measurement: A review. J. Quant. Spectrosc. Radiat. Trans. 110, 844–878.

Rannou, P., Cours, T., Le Mouélic, S., Rodriguez, S., Sotin, C., Drossart, P., Brown, R., 2010. Titan haze distribution and optical properties retrieved from recent observations. Icarus 208, 850–867. http://dx.doi.org/10.1016/j.icarus.2010.03.016.

Sittler, E.C. et al., 2009. Heavy ion formation in Titan's ionosphere: Magnetospheric introduction of free oxygen and a source of Titan's aerosols? Planet. Space Sci. 57, 1547–1557. http://dx.doi.org/10.1016/j.pss.2009.07.017.

Tomasko, M.G. et al., 2005. Rain, winds and haze during Huygens probe's descent to Titan's surface. Nature 438 (8), 765–778.

Tomasko et al., 2008. A model of Titan's aerosols based on measurements made inside the atmosphere. Planet. Space Sci. 56, 669–707.

Tran et al., 2003. Simulation of Titan haze formation using a photochemical flow reactor: The optical constants of the polymer. Icarus 165, 379–390.